 CMES, vol.82, no.4, pp.253-264, 2011

Creation of Imperfections for Welding Simulations

L. Novotný[1] **and M. Tsunori**[2]

Abstract: The welding simulation is carried out by an uncoupled thermal and mechanical analysis or by a coupled thermo–mechanical analysis. For weld–induced distortion and residual stress simulation, nonlinear mechanical analysis is required. Nonlinearities are caused by both nonlinear behaviour of the material and geometrical nonlinearity. Usually, the element birth technique is used to incorporate the filler material in the model. The ideal straight geometry may be altered by imperfections to enable buckling behaviour. Real component shapes contain various imperfections (e.g. geometrical, material). The finite element mesh may contain geometrical imperfections too. When a simple weld model is used, the mode of the end–distortion is predictable. The imperfections are created in the same shape as predicted. The sufficient magnitude of an imperfection is approximately 1/100 of end–distortion. In case that complex weld model shapes are used, it is not easy to predict the correct imperfection shape. For general purpose as well, the common procedure for calculation of correct imperfections shapes is required. In these article a new approach to create imperfections was adopted. The results obtained in the course of this work allowed to calculate resultant welding distorsion more accurate.

Keywords: Imperfection, finite element method, welding simulation, thermal analysis.

1 Problem description, finite element model without imperfection

Next finite element simulations represent real welding experiment. In a trial, two plates of dimensions 500 mm long, 250 mm wide and 4 mm thickness were single pass butt welded. Steel plates were welded using gas metal arc welding [Davies, Wimpory, Béreš, Lightfoot, Dye, Oliver, O'Dowd, Bruce and Nikbin, (2007)]. The

[1] Faculty of mechanical engineering, Technical university in Košice, Letná 9, 04200 Košice, Slovakia, e-mail: ladislav.novotny@gmail.com

[2] Structure and Strength Department, Research Laboratory, IHI corporation 1, Shin-Nakahara-cho, Isogo-ku, Yokohama, JAPAN, 235-8501, mitsuyoshi_tsunori@ihi.co.jp

material chosen for the base plate was a high strength low alloy DH–36 steel. Convection filler material weld wires (1 mm in diameter) were used; which undergoes solid–state phase transformation at a relatively high temperature, 560 ˚C. The chemical compositions of the plates and the weld consumables are shown in Table 1. During manual welding the plates were rested, unclamped, on wooden pallets. They were held 4 mm apart by series of approximately 25 mm long tack welds at three locations with intervals of approximately 220 mm. A ceramic backing tile was used to contain the weld pool.

Table 1: T Chemical composition (wt. %) of steel plate and weld wire

	C	Si	Mn	P	S	Cu	Ni	Cr	Nb
steel plate	0.11	0.18	1.29	0.01	0.004	0.02	0.03	0.03	0.01
weld wire	0.07	0.61	1.42	0.01	0.01	0.14	0.04	0.02	0.02

The welding conditions employed was: weld speed v =2.7 mm s^{-1}, weld current I =150 A, weld voltage U =18 V, heat input H =1.0 kJ mm^{-1} [Tsunori, M.; Davies, C. M.; Dye, D.; Nikbin, K. M. (2008)].

2 Finite element model without imperfection – Model 0

Finite element mesh contains 21200 elements (20 nods 3D volume elements) and 102823 nods.

In the vicinity of the weld, an uniform refined mesh was used as can be seen in Fig.1(c). Symmetry boundary conditions were defined to the nods on face of symmetry.

Moving heat flux was considered on the surface of elements along the weld line

$$h = \frac{\eta IU}{A},$$

where η =0.75 is thermal efficiency of welding, A is area of torch arc surface, (I is the weld current, U is the voltage). The Von Misses elastic–plastic material law with kinematic hardening was used. Temperature depended material properties were employed in the calculations (Fig. 2).

Heat transfer analysis was performed with fixed time increment. Newmark method was used in solution. The next mechanical analysis used time depended of temperature field from heat transfer analysis. Newton-Raphson solution technique was used in calculations.

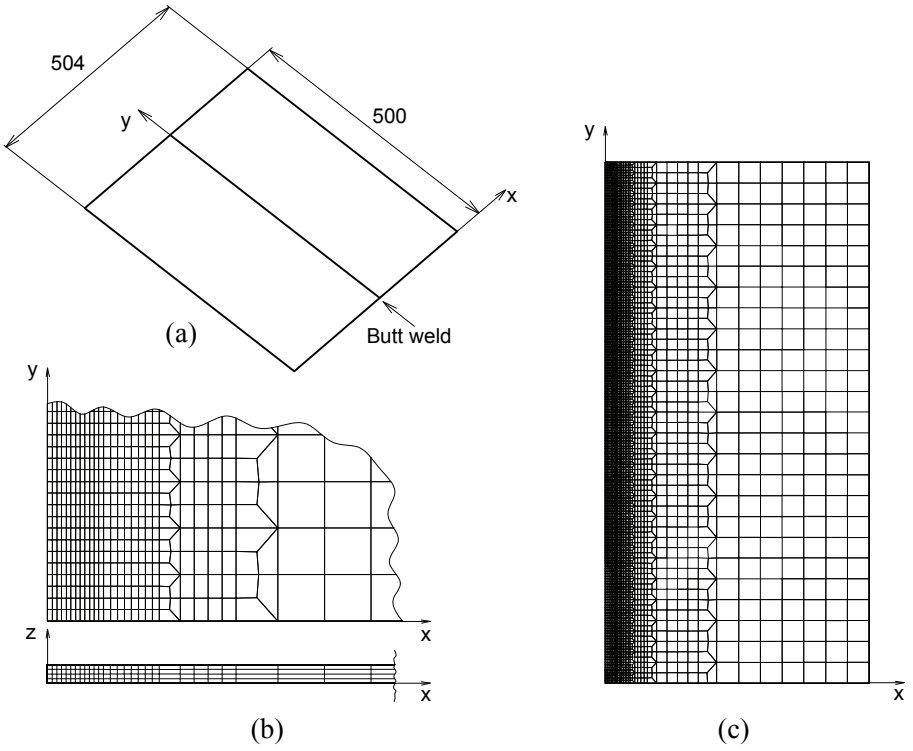

Figure 1: a) Schematic illustration of the butt welded plate b) Detail of finite element mesh c) Finite element mesh

Temperature field is time depended. Place of maximal value of temperature is moving with conjunction of moving of prescribed heat flux, as shownin the Fig. 3(a)– temperature field in time 135.2 s. On the Fig. 3(b) the end–displacement after welding and cooling is presented (mirrored results).

3 Models with imperfections

The mode and the magnitude of the imperfection is crucial when buckling behavior of thin structures during welding is studied. For complex shape of welded structure the next approach was used for imperfection creation. The result mode shape from linear buckling analysis was used as imperfection. Load for linear buckling analysis was shrinkage in weld line in linear mechanical analysis. Load for linear mechanical analysis was simplified temperature field. Simplified temperature field

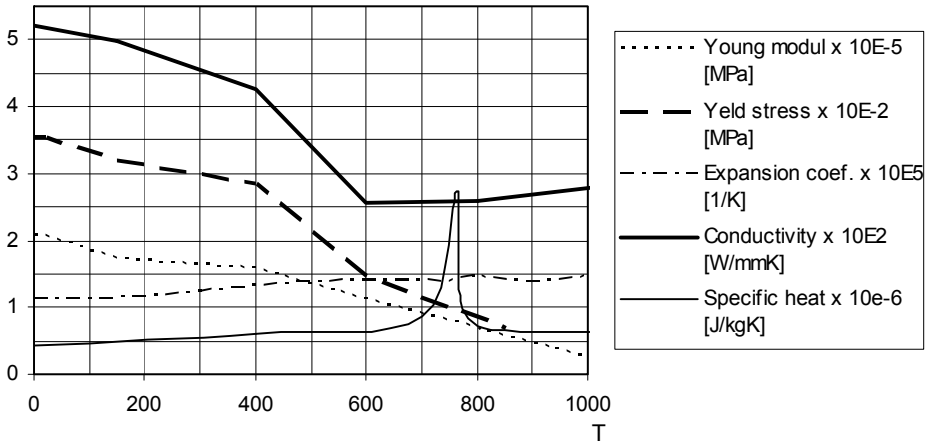

Figure 2: Material properties

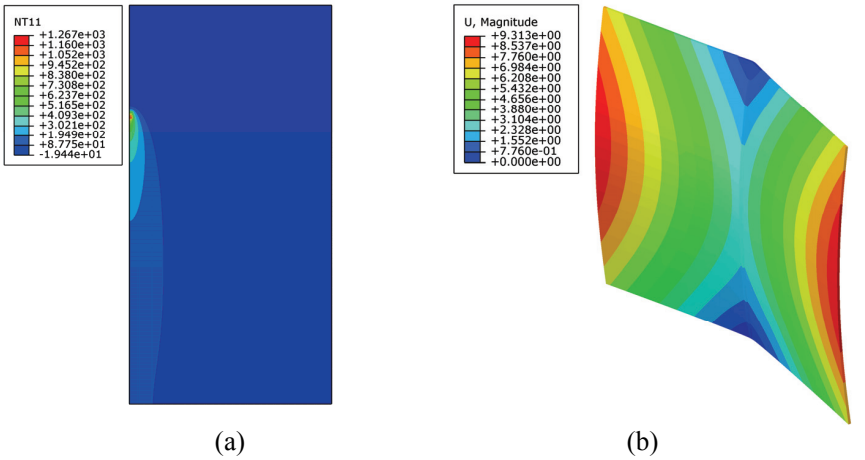

(a) (b)

Figure 3: a) Temperature field during welding in simulation b) End-displacement

was created by prescribe low temperature value to node in weld line compare with others nodes.

3.1 Linear buckling analysis in principle

The linear combination of mode shapes from linear buckling analysis can be used as the imperfection shape for the nonlinear analysis.

When we include the initial stress stiffness matrix–nonlinear system (in part)

$$(\mathbf{K}+\mathbf{K}_\sigma)\,\mathbf{d}=\mathbf{f}.$$

At the critical (buckling) condition there is bifurcation in load versus displacement plot. Two infinitesimally close equilibrium states are possible–the unbuckled state and the buckled state–without any change in applied loads F

$$(\mathbf{K}+\lambda\mathbf{K}_\sigma)\,d\mathbf{d}=\mathbf{0}.$$

The linear buckling analysis refers to generalized eigenvalue problem

$$(\mathbf{K}+\lambda\mathbf{K}_\sigma)\,\mathbf{r}=\mathbf{0}.$$

Trivial solution $\mathbf{r}=\mathbf{0}$ for any value of λ is not interesting. Nontrivial solutions $\mathbf{r}_i\neq\mathbf{0}$ are only if

$$\det(\mathbf{K}+\lambda\mathbf{K}_\sigma)=0. \tag{1}$$

This is an n–th order of λ, from which we can find n solutions (roots) or eigenvalues λ_i. For each λ_i Eq. 1 have one solution (eigenvector)

$$(\mathbf{K}+\lambda_i\mathbf{K}_\sigma)\,\mathbf{r}_i=\mathbf{0},$$

where

λ_i is the factor by which this level must be increased or decreased in order to produce buckling (for i–order eigenshape),

$\mathbf{r}_i$ is normal mode–mode shapes (for i–order eigenvalue),

$\mathbf{K}$ is conventional stiffness matrix,

$\mathbf{K}_\sigma$ is stress stiffness matrix (initial stress stiffness matrix, geometric stiffness matrix, differential stiffness matrix, stability coefficient matrix, etc.),

$\mathbf{d}_i$ is vector of nodal d.o.f. (for i–order eigenvalue),

$\mathbf{f}$ is vector of applied load.

For computing only the significant eigenvalues and eigenvectors, the shift s can be used

$$(\mathbf{K}+(\lambda_i-s)\mathbf{K}_\sigma)\,\mathbf{r}_i=\mathbf{0}.$$

Mode shapes are orthogonal to each other with respect $\mathbf{K}$ and $\mathbf{K}_\sigma$ matrices

$$\mathbf{r}_i^{\mathrm{T}}\mathbf{K}\mathbf{r}_j=1,$$

$$\mathbf{r}_i^{\mathrm{T}}\mathbf{K}_\sigma\mathbf{r}_j=\lambda.$$

3.2 Calculation of imperfections for welding simulations

3.2.1 Linear steady state thermal analysis

The uniform lower temperature load was prescribed to the nods of elements represented of welded material. The uniform higher temperature load was prescribed to the nods of plate material. Magnitude of both the higher temperature and the lower temperature is irrelevant, because in the linear buckling analysis the eigenvectors will be normed. The temperature load was prescribed to all nods of the model, but in addition the linear steady state thermal analysis was required for the creation of the thermal matrix (thermal load) for the following mechanical calculation (stress calculation).

3.2.2 Linear mechanical analysis

The thermal load from the linear steady state thermal analysis was used to calculate the shrinkage in welded part.

Magnitude of shrinkage was irrelevant, too (because in the linear buckling analysis the eigenvectors were normed). Symmetrical boundary conditions were prescribed along the welding line. The purpose of this calculation was the creation of the initial stress stiffness matrix for the following linear buckling analysis.

3.2.3 Linear buckling analysis, models with imperfections

The first twenty eigenvectors and eigenvalues were calculated. To compute the first nonnegative eigenvectors and the subsequent eigenvalues, shift in the magnitude $s = 13$ was used. The first twenty eigenshapes are presented in Fig. 5. The eigenshapes are normed, and then the imperfections are created as the multiple of the subsequent mode shape displacements. Multiple factor can be expressed

$$c_i = \frac{u_i^{\mathrm{Imp}}}{u_i^{\mathrm{Norm}}},$$

where

c_i is multiple factor for i–th mode shape,

u_i^{Imp} is maximal value of displacement in i–th mode shape imperfection,

u_i^{Norm} is maximal value of displacement in i–th normed mode.

The final imperfection can be created as a linear combination of several mode shapes displacements. Nodal coordinates were updated by the imperfections

$$\mathbf{x}^{\mathrm{IMP}} = \mathbf{x} + c_i \mathbf{r}_i,$$

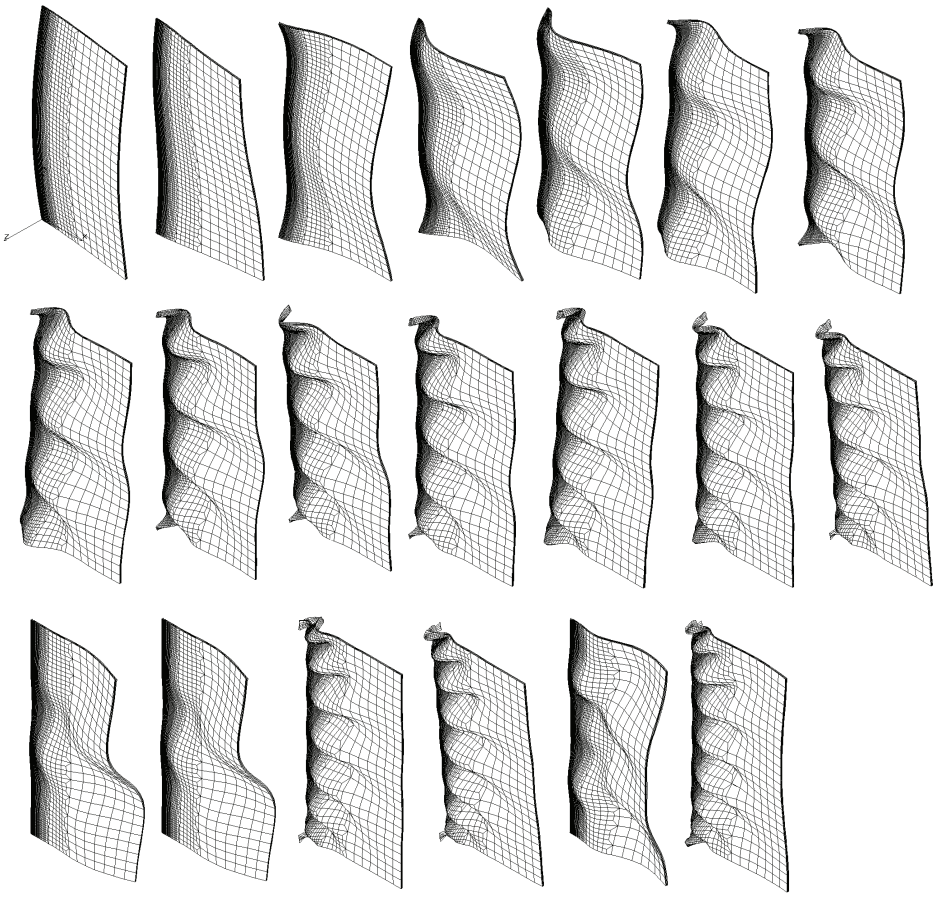

Figure 4: Various modes of eigenshapes

where

$\mathbf{x}^{\mathrm{IMP}}$ is vector of nodal coordinates with imperfections,

$\mathbf{x}$ is vector of nodal coordinates without imperfections,

$\mathbf{r}_i$ is normed modes–mode shapes (for i–order eigenvalue).

By this approach, the imperfections were added to the nodes coordinates.

3.3 Models with imperfections

Three different models with imperfections were created and these varied in number of mode shapes included and in scale of included mode shapes.

Model 1

This model contained only the first mode shape. Maximal mode shape displacement was $u_1^{\text{Imp}} = 0.5\text{mm}$ (maximal total imperfection was 0.5 mm). Multiple factor $c_1 = 3.4409194$.

Model2

Maximal mode shapes displacements were 0.5mm (maximal total imperfections were 0.5 mm) for each of the mode shapes

$$u_1^{\text{Imp}} = u_2^{\text{Imp}} = u_3^{\text{Imp}} = u_4^{\text{Imp}} = u_5^{\text{Imp}} = 0.5\text{mm}.$$

Model3

This model contained the first twenty mode shapes. Maximal mode shape displacement of the first mode shape was 0.5 mm

$$u_1^{\text{Imp}} = 0.5\text{mm}.$$

Maximal mode shape displacement for the following mode shapes was described by the formula

$$u_i^{\text{Imp}} = \frac{\left|u_1^{\text{Imp}}\right|}{\lambda_i}.$$

Subsequent maximal mode shape displacements was

$$u_1^{\text{Imp}} = 0.5, \quad u_2^{\text{Imp}} = 0.2483, \quad u_3^{\text{Imp}} = 0.1639, \quad u_4^{\text{Imp}} = 0.1196, \quad u_5^{\text{Imp}} = 0.09199,$$

$$u_6^{\text{Imp}} = 0.07435, \quad u_7^{\text{Imp}} = 0.06184, \quad u_8^{\text{Imp}} = 0.0525, \quad u_9^{\text{Imp}} = 0.04526,$$

$$u_{10}^{\text{Imp}} = 0.03953, \quad u_{11}^{\text{Imp}} = 0.0349, \quad u_{12}^{\text{Imp}} = 0.03112, \quad u_{13}^{\text{Imp}} = 0.02798,$$

$$u_{14}^{\text{Imp}} = 0.02536, \quad u_{15}^{\text{Imp}} = 0.02455, \quad u_{16}^{\text{Imp}} = 0.0245, \quad u_{17}^{\text{Imp}} = 0.0231,$$

$$u_{18}^{\text{Imp}} = 0.02126, \quad u_{19}^{\text{Imp}} = 0.01977, \quad u_{20}^{\text{Imp}} = 0.01967.$$

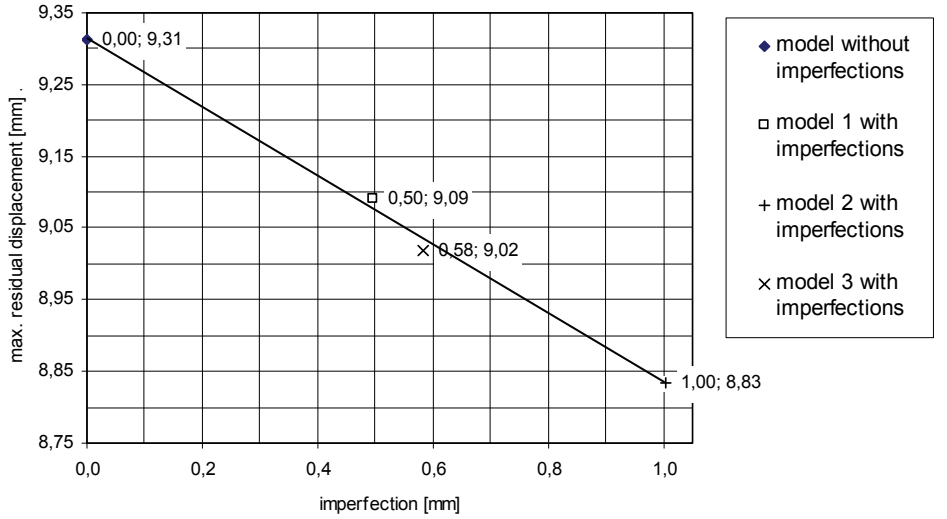

Figure 5: Behaviour of resultant welding displacement on the maximum initial imperfection

4 Welding simulations by models with imperfections, calculation results

An equal welding parameter and calculation control as in welding model without imperfections was used. Only the mesh was different (coordinates of nodes and elements definitions). The maximal values of resultant displacements for each model are shown in Fig. 5.

Fig. 5 illustrates that the resultant welding displacement decreases with increasing of initial imperfection (a sum of imperfections of particular mode shapes in the relevant model).

Fig. 6 shows the dependence of displacements for particular models with imperfections along the outer edge (parallel with welding line).

The small differences are also in place of maximal value of displacements. The differences are not only in magnitudes, but also in shapes. Differences between the results of model without imperfection and the results of model with imperfection were calculated as

$$\Delta u_{im} = u_{im}^{\text{Model With Imp}} - k_{im} \cdot u^{\text{Model Without Imp}},$$

$$\Delta u_{im} = u_{im}^{\text{Model With Imp}} - \frac{\int_l u_{im}^{\text{Model With Imp}} \, \mathrm{d}l}{\int_l u^{\text{Model Without Imp}} \, \mathrm{d}l} \cdot u^{\text{Model Without Imp}},$$

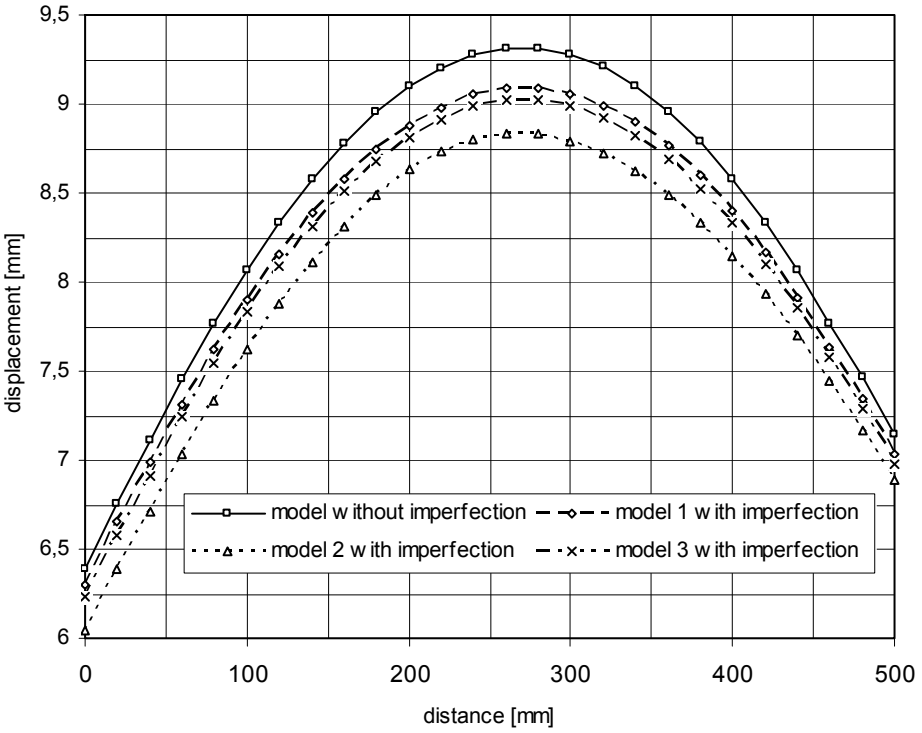

Figure 6: Resulting deformation along the outer edge

where im is the number of model with imperfection ($im = 1,2,3$), $u_{im}^{\text{Model With Imp}}$ are the results of displacements on im–th model with imperfection, $u^{\text{Model Without Imp}}$ are the results of displacements on model without imperfection, l is the line along the outer edge (parallel with welding line).

Resultant differences in displacement for each models with imperfection compare with model without imperfection are shown in Fig. 7. Calculated parameters for comparing were $k_1 = 0.97915$, $k_2 = 0.94876$, $k_3 = 0.97082$.

There is a zero plastic deformation in the part of body around the outer edge; behaviours in Fig. 7 are smooth functions.

5 Conclusion

A new approach to create imperfections for welding simulations was adopted. These include calculations of imperfections as linear combinations of mode shapes,

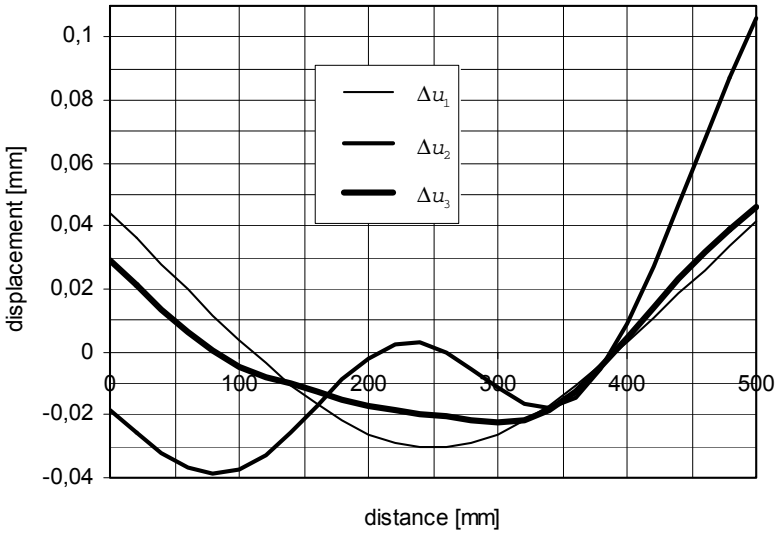

Figure 7: Differences between the results of displacements along the outer edge

mode shapes were calculated in linear buckling analysis. In the weld model with simple geometry, the imperfections are not necessary. They are useful in models with more complex shapes. The first non–zero eigenvalue mode shape is the most significant for imperfections. Imperfection mode shapes of higher order must be included in the imperfections with a declining multiplier. The consideration of greater number of imperfection mode shapes in the analysis can make the calculation more accurate.

References

Béreš, M.; Abreu, H.; Davies, C. M.; Dye, D. (2010): The observation of variant transformations in the fusion zones of Gas Metal Arc Welds. In preparation for submission to *Materials Science and Engineering*.

Bhadeshia, H. K. D. H. (1998): Modelling of Phase Transformations in Steel Weld Metal. Proceedings of *ECOMAP '98 (Environment Concious Innovative Materials Processing)*, Kyoto, Japan, published by the High Temperature Society of Japan, pp. 35-44.

Davies, C. M.; Wimpory, R. C.; Béreš, M.; Lightfoot, M. P.; Dye, D.; Oliver, E.; O'Dowd, N. P.; Bruce, G. J.; Nikbin, K. M. (2007): The Effect of Residual Stress and Microstructure on Distortion in Thin Welded Steel Plates. *Proceedings*

of PVP2007 ASME Pressure Vessels and Piping Division Conference, July 22-26, San Antonio, Texas.

Deng, D.; Murakawa, H. (2007): Prediction of welding distortion and residual stress in a thin plate butt-welded joint. *Computational Materials Science*, 2008, 43(2), pp. 353-365.

Masubuchi, K. (1980): Analysis of welded structures: residual stresses, distortion, and their consequences. *Pergamon Press*, Oxford.

Novák, P.;Meško, J.; Žmindák, M. (2009): Thermal cycle and residual stresses in weld deposite. In *Machine modeling and simulations*. Žilina.

Tsunori, M.; Davies, C. M.; Dye, D.; Nikbin, K. M. (2008): Numerical Modelling of Residual Stress and Distortion in Thin Welded Steel Plates, in Proceedings of PVP2008 *ASME Pressure Vessels and Piping Division Conference*, July 27th-31st 2008, Chicago, Illinois, USA.